Title

A Protein-Based Biosensor for Detecting Calcium by Magnetic Resonance Imaging

Journal

ACS Sensors, 6(9)

ISSN

2379-3694

Authors

Ozbakir, Harun F
Miller, Austin DC
Fishman, Kiara B
et al.

Publication Date

2021-09-24

DOI

10.1021/acssensors.1c01085

Peer reviewed

HHS Public Access

Author manuscript

ACS Sens. Author manuscript; available in PMC 2022 June 12.

Published in final edited form as:

ACS Sens. 2021 September 24; 6(9): 3163–3169. doi:10.1021/acssensors.1c01085.

A Protein-Based Biosensor for Detecting Calcium by Magnetic Resonance Imaging

Harun F. Ozbakir,
Department of Chemical Engineering, University of California, Santa Barbara, California 93106, United States

Austin D. C. Miller,
Biomolecular Science and Engineering, University of California, Santa Barbara, California 93106, United States

Kiara B. Fishman,
Department of Molecular, Cellular, and Developmental Biology, University of California, Santa Barbara, California 93106, United States

André F. Martins,
Werner Siemens Imaging Center, Department of Preclinical Imaging and Radiopharmacy and Cluster of Excellence iFIT (EXC 2180) “Image-Guided and Functionally Instructed Tumor Therapies”, Eberhard Karls University of Tübingen, Tübingen 72076, Germany;

Tod E. Kippin,
Neuroscience Research Institute and Psychology and Bran Sciences, University of California, Santa Barbara, California 93106, United States

Arnab Mukherjee
Department of Chemical Engineering, Biomolecular Science and Engineering, Department of Chemistry, Neuroscience Research Institute, and Center for Bioengineering, University of California, Santa Barbara, California 93106, United States;

Abstract

Corresponding Author: Arnab Mukherjee – Department of Chemical Engineering, Biomolecular Science and Engineering, Department of Chemistry, Neuroscience Research Institute, and Center for Bioengineering, University of California, Santa Barbara, California 93106, United States; Phone: (805) 893-5137; arnabm@ucsb.edu.

Author Contributions

AM conceived the study. HFO and AM designed experiments with inputs from AFM and TEK. HFO performed all experiments with help from ADCM and KBF who assisted in biochemical studies. HFO and AM analyzed data and wrote the manuscript with inputs from all authors. AM supervised the research.

Supporting Information

The Supporting Information is available free of charge at https://pubs.acs.org/doi/10.1021/acssensors.1c01085.

Figures depicting biochemical purification and functional validation of calprotectin, analyte-induced percent change in relaxation times for published metalloprotein-based MRI sensors, relaxometric titration of His_3Asp variant in the presence and absence of calcium, voxel-wise T_1 and T_2 response of calprotectin-based calcium sensor, calcium imaging in HT-22 cell lysates, Mn^{2+} uptake and toxicity in model mammalian cells, calcium imaging in CHO cells transduced with calprotectin and treated with a Ca^{2+} ionophore (calcimycin); tabulated values of Mn^{2+} binding affinity, and MRI response of published nongenetic calcium sensors, materials and methods; gene sequences of all constructs used in this work (PDF)

Complete contact information is available at: https://pubs.acs.org/10.1021/acssensors.1c01085

The authors declare no competing financial interest.

Calcium-responsive contrast agents for magnetic resonance imaging (MRI) offer a promising approach for noninvasive brain-wide monitoring of neural activity at any arbitrary depth. Current examples of MRI-based calcium probes involve synthetic molecules and nanoparticles, which cannot be used to examine calcium signaling in a genetically encoded form. Here, we describe a new MRI sensor for calcium, based entirely on a naturally occurring calcium-binding protein known as calprotectin. Calcium-binding causes calprotectin to sequester manganese ions, thereby limiting Mn^{2+} enhanced paramagnetic relaxation of nearby water molecules. We demonstrate that this mechanism allows calprotectin to alter T_1 and T_2 based MRI signals in response to biologically relevant calcium concentrations. The resulting response amplitude, i.e., change in relaxation time, is comparable to existing MRI-based calcium sensors as well as other reported protein-based MRI sensors. As a preliminary demonstration of its biological applicability, we used calprotectin to detect calcium in a lysed hippocampal cell preparation as well as in intact Chinese hamster ovary cells treated with a calcium ionophore. Calprotectin thus represents a promising path toward noninvasive imaging of calcium signaling by combining the molecular and cellular specificity of genetically encodable tools with the ability of MRI to image through scattering tissue of any size and depth.

Graphical Abstract

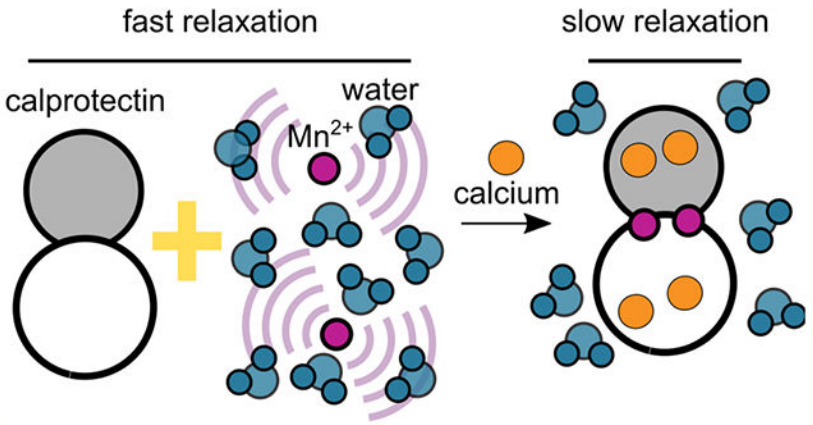

Keywords

magnetic resonance imaging; calcium imaging; genetically encoded reporters; neuroimaging; Mn^{2+} enhanced MRI

In the nervous system, calcium ions give rise to intracellular signals that modulate a wide range of biological functions including neural activity, gene expression, synaptic communication, and apoptosis.[1,2] Consequently, experimental imaging of calcium in living cells and organisms is a cornerstone technology for obtaining detailed, time-lapse information on neural signaling mechanisms.[3–5] High-resolution calcium imaging typically relies on fluorescent dyes and genetically encoded calcium indicators (GECIs), which in conjunction with multiphoton microscopy can detect activity in single cells up to depths of 1 mm in intact tissue.[6–16] However, the imaging volume typically accessible by optical methods (~1 mm^3) encompasses only a small fraction of the brain in most vertebrates.[17–20]

Calcium signals can also be recorded from deeper tissues using endoscopes and specialized lenses, but these techniques cover a limited field of view and require invasive surgery to embed the imaging hardware inside tissues.[21,22] Among noninvasive modalities, magnetic resonance imaging (MRI) is unrivaled in its ability to access large volumes of intact tissue located at any arbitrary depth. Thus, MRI-based calcium sensors have the potential to uniquely complement optical indicators by enabling wide-field imaging of biological processes in deep tissues noninvasively. This vision has motivated the development of a versatile collection of small-molecule paramagnetic complexes, fluorinated agents, and superparamagnetic iron oxide crystals that have evolved over the past two decades for imaging calcium by various MRI mechanisms including longitudinal (T_1) and transverse (T_2) relaxation, chemical exchange saturation transfer (CEST), and direct detection of ^{19}F spins.[23–40] Regardless of the specific contrast mechanism, all reported MRI probes for calcium are synthetic molecules, which makes them incompatible with genetic technologies for *in vivo* delivery, stable long-term expression, and cell type specific targeting—key aspects that underpin the prolific success of genetically encoded calcium indicators derived from the green fluorescent protein (GFP).[10] While iron-containing enzymes such as cytochrome P450 and ferritin nanoparticles have been used to develop protein-based MRI sensors for functional imaging of neurotransmitters and kinase activity,[41–46] to the best of our knowledge, there are no reported examples of protein-based MRI probes for calcium imaging. Here, we describe the development of the first biomolecular MRI reporter for calcium, based on a novel manganese metalloprotein, and demonstrate its utility for imaging calcium in a biological context.

RESULTS AND DISCUSSION

Our sensor is based on calprotectin, an antimicrobial protein that is released by neutrophils to chelate essential transition metals (including paramagnetic Mn^{2+} ions), thus limiting their availability for pathogenic microorganisms in infection sites.[47–50] The calprotectin heterodimer coordinates Mn^{2+} using two histidine-rich motifs located at the interface of the two subunits.[48,51–53] Each subunit also contains a canonical EF-hand motif for binding calcium.[54] Early biochemical studies on calprotectin found that calcium ions are responsible for tuning its Mn^{2+} binding properties, allowing the protein to strongly bind Mn^{2+} ions only when calcium ions are also bound.[52,55,56] Based on calprotectin's unique ability to sequester Mn^{2+} ions and shield them from nearby water molecules specifically in response to calcium, we reasoned that it should be possible to adapt calprotectin for MRI-based detection of calcium. Specifically, we hypothesized that in the absence of calcium, a binary mixture of calprotectin and Mn^{2+} ions would effectively shorten the T_1 and T_2 relaxation times of water molecules due to paramagnetic relaxation enhancement from free (i.e., unbound) Mn^{2+}. In the presence of calcium, calprotectin would sequester free Mn^{2+} ions, limiting access to neighboring water molecules and consequently increase relaxation times in inverse proportion to the concentration of free Mn^{2+} ions remaining in solution (Figure 1A). To test our hypothesis, we cloned both subunits of human calprotectin in *E. coli* BL21 cells, substituting the single cysteine residue in each subunit with serine to avoid cross-linking during purification. We purified and reconstituted the 26 kDa heterodimer using metal-affinity chromatography and verified biochemical function by assaying for

calcium-dependent Mn^{2+} binding using a fluorescent dye (Figure S1). Next, we incubated various concentrations of purified calprotectin with Mn^{2+} and measured changes in T_1 and T_2 relaxation times at high (7 T) magnetic field induced by saturating amounts (~50-fold excess) of calcium. These experiments revealed a calcium-dependent increase in relaxation times ranging from 20 ± 4% to 95 ± 4% for T_1 and 56 ± 14% to 201 ± 2% for T_2 ($N = 5$) (Figure 1B), thereby allowing calcium ions to be respectively visualized as darkening or brightening of MRI signals in standard T_1 and T_2 weighted images (Figure 1C). Relaxivity values of the Mn^{2+}-bound protein complex in the presence of calcium were measured as 0.20 ± 0.07 mM^{-1} s^{-1} (r_1) and 3.30 ± 0.33 mM^{-1} s^{-1} (r_2), which are substantially smaller than free Mn^{2+} relaxivity.[57] The lower relaxivity of Mn^{2+} in the bound state is consistent with previous studies that found the Mn^{2+} coordination environment in calprotectin to largely exclude water molecules.[55] Notably, the amplitude of T_1 and T_2 changes obtained with calprotectin are 2–6-fold larger than the peak response estimated for identical concentrations of metal-loprotein-based MRI sensors (targeting dopamine,[42] serotonin,[44] protein kinase[41]) reported to date (Figure S2). To characterize calprotectin's contrast mechanism in greater detail, we performed relaxometric titrations by treating calprotectin with a range of Mn^{2+} concentrations and measuring T_1 and T_2 values in the presence or absence of excess calcium. In calcium-free conditions, we observed a consistent decrease in T_1 as the amount of Mn^{2+} was increased from 0 to 40 μM (corresponding to 0–1 molar equiv protein). In contrast, when calcium ions were present, the extent of T_1 change was significantly smaller ($p < 0.01$, $N = 5$) in the range of 10–40 μM Mn^{2+} (Figure 2A). We detected a similar trend in T_2 values, which decreased with increasing concentrations of Mn^{2+} in the absence of calcium but displayed a significantly smaller change when calcium ions were available (Figure 2B). By fitting the measured T_1 changes to binding isotherms, we determined that calcium elicits ~35-fold increase (K_d(−Ca) = 49.7 ± 8.0 μM, K_d(+Ca) = 1.42 ± 0.42 μM, $p = 0.0003$, $N = 5$) in calprotectin's binding affinity for Mn^{2+}, consistent with results from previous spectroscopic and calorimetric studies (Figure 2C and Table S1).[52,56] To further probe calprotectin's MRI properties, we introduced alanine substitutions in calprotectin's histidine-rich motifs to examine whether the calcium response is altered by changes in the Mn^{2+} coordination environment.[52,54,55] We examined the resulting variants using relaxometry (Figure S3) and found one mutant ($His_3Asp \rightarrow Ala_4$) that displayed lower Mn^{2+} affinity in the calcium-free state (K_d = 184.3 ± 43.6 μM) relative to wild-type calprotectin, leading to a modest but statistically significant increase ($N = 3$, $p = 0.005$) in overall calcium-induced fold change in relaxation time (Figure 2C,D and Table S2). Finally, we assessed the selectivity of calprotectin's MRI response toward calcium by incubating a mixture of calprotectin and Mn^{2+} ions with magnesium (50-fold excess), representing the most abundant divalent cation found in cells. No significant change in T_1 or T_2 values could detected under these conditions ($p \geq 0.2$, $N = 4$) (Figure 2E,F). Next, we established the dynamic range over which calcium ions can be sensed by calprotectin. For these experiments, we fixed the amount of calprotectin and Mn^{2+} at 40 and 30 μM, respectively, and measured T_1 and T_2 changes in buffered solutions consisting of calprotectin titrated with varying concentrations of calcium. In these settings, we detected an 18.7 ± 2.5% ($p = 0.007$, $N = 3$) increase in T_1 and a 77.5 ± 1.5% ($p = 1.0 \times 10^{-4}$, $N = 3$) increase in T_2 over calcium concentrations spanning the full biologically relevant range of (0.1–100 μM) (Figures 3A and S4). Taken together, our results indicate that calprotectin can be used to

detect biologically relevant calcium changes based on an increase in T_1 and T_2 relaxation times triggered by calcium-induced binding to free Mn^{2+}, which leads to their sequestration in a low relaxivity state.

Next, as a precursor to calcium imaging in mammalian cells, we examined the sensor's calcium response in cellular conditions using intracellular lysates prepared from a mouse hippocampal cell line (HT-22). Similar cell lysate preparations have been previously used for *in vitro* validation of protein-based MRI sensors.[41] We supplemented the cell lysate with purified calprotectin and manganese chloride and then measured changes in relaxation times following treatment with calcium concentrations relevant to neural activity. In this cellular milieu, calcium concentrations as low as 5 μM were found to induce a significant increase in T_1 (7.0 ± 1.8%, $p = 0.02$, $N = 4$) and T_2 (9.1 ± 1.0%, $p = 0.0015$, $N = 4$) (Figure 3B), while no change was detected when calcium was added to control lysates containing Mn^{2+} but lacking calprotectin ($p > 0.2$, $N = 3$) (Figure S5). Importantly, the T_1 and T_2 changes obtained with calprotectin are comparable to the calcium response reported for existing Gd^{3+} and Mn^{3+} based calcium probes (Table S3) and correspond to signal amplitudes that can be reliably detected *in vivo* by MRI techniques[35,42,45,58] already established for functional brain imaging.

Finally, we incorporated calprotectin in a polycistronic lentiviral construct, which was used to transduce a Chinese hamster ovary (CHO) cell line to establish stable expression from a strong CMV promoter. We delivered Mn^{2+} to cells by direct supplementation in the culture medium (Figure S6) and stimulated calcium entry by the addition of a calcium ionophore (calcimycin) in the presence or absence of extracellular calcium (5 mM). We performed T_1 measurements on pelleted cells based on procedures established in our earlier work.[59] To control for nonspecific T_1 changes arising from ionophore treatment, wild type CHO cells were also treated with calcimycin and imaged concurrently under identical conditions. In the presence of calcium, calprotectin-expressing cells were found to exhibit a 22 ± 4% increase in T_1 compared to control cells ($p = 0.011$), whereas no change in T_1 could be detected when either calcium or calcimycin was omitted from the medium ($p > 0.7$) (Figures 3C and S7). Taken together with our results from the hippocampal preparation, these observations indicate that calprotectin may be used for MR imaging of calcium activity to detect changes from the resting-state (~50–100 nM in neurons) to tens of micromolar concentration, which may be reached in stimulation paradigms involving electrical neuromodulation,[60] seizures,[61,62] and excitotoxic injury.

CONCLUSIONS

Our findings represent the first example of a genetic construct for imaging calcium with MRI. The observed changes in T_1 and T_2 relaxation in response to calcium binding are comparable to most synthetic calcium probes (Table S3) and exceed that of previous protein-based MRI biosensors (Figure S2). Future work will focus on expressing calprotectin in neuronal cell lines, primary neurons, and eventually *in vivo*, which will allow whole-brain imaging of calcium activity with the added benefit of being able to probe specific cell populations by genetic targeting. To this end, a preliminary assessment of the feasibility of applying calprotectins *in vivo* may be drawn by comparing with ManICS1, a synthetic

(i.e., nongenetic) Mn^{2+} based calcium probe that was recently used to obtain the first measurements of intracellular calcium signals by MRI.[35] In this work, brain regions were acutely loaded with ManICS1 and stimulated by K^+ infusion, which elicited a maximum T_1 weighted signal change of 5.8 ± 1.2%. Notably, both ManICS1 and calprotectin exhibit similar IC_{50} values for calcium binding (Table S3 and Figure 3A). However, calcium binding induces a larger relaxivity change in the calprotectin/Mn^{2+} sensor system (5.6 to 0.2 mM^{-1} s^{-1}) compared to ManICS1 (3.6 to 5.1 mM^{-1} s^{-1}). Given the successful implementation of ManICS1 for *in vivo* imaging, we therefore think that it should be possible in principle to adapt calprotectin-based sensors for imaging of calcium signals in the brain. However, practical challenges related to Mn^{2+} transport, background relaxation in brain tissue, reporter gene expression, and detection sensitivity will need to be addressed. Accordingly, we envision several areas of future development related to the application of calprotectins in animal models. First, Mn^{2+} dosing should be carefully optimized to minimize toxicity as well as ensure effective delivery to brain regions of interest. Several techniques for transporting Mn^{2+} (typically in quantities of tens of nanomoles, corresponding to intracellular concentrations of 35–93 μM in the rodent brain[63]) with minimum acute toxicity have already been established in the context of Mn^{2+} enhanced MRI (MEMRI). These techniques include oral delivery, intraperitoneal administration, systemic injection, transcranial diffusion, and direct infusion in the cerebrospinal fluid.[64–66] Although Mn^{2+} can passively enter the brain parenchyma, transient and reversible opening of the blood brain barrier (e.g., using focused ultrasound) may be employed to augment the amount of Mn^{2+} transported.[67] A second challenge also related to Mn^{2+} delivery involves cell-type dependent variations in Mn^{2+} transport as well as increased Mn^{2+} flux (through calcium channels) in response to neural activity. The latter mechanism in fact serves as the basis for mapping activated brain regions by a technique known as activity-induced Mn^{2+} dependent MRI (AIM).[68–70] One potential approach for offsetting variabilities arising from cell-specific and activity-dependent changes in Mn^{2+} movement could be to co-express calprotectin with DMT1, a Mn^{2+} transporter, which is also used as an MRI reporter based on its ability to constitutively transport Mn^{2+} in cells.[71,72] Furthermore, because intracellular Mn^{2+} clears slowly from the brain (on the order of days), it may be feasible to implement calprotectins in conjunction with AIM. This could be done by time-locking calprotectin expression (e.g., using Cre-lox or TetTag transgenic models) to a temporal window that follows the AIM segment without further Mn^{2+} infusion. With judicious controls as well as detailed knowledge of calprotectin's response kinetics, such a multiparametric approach to functional MRI could reveal complementary insights on brain activity. Finally, although T_1 weighted signal changes as small as ~1% have been reliably measured *in vivo* using protein-based neurotransmitter sensors,[42,45,58] statistical fidelity of calcium detection can be greatly enhanced by optimizing calprotectins for a larger response amplitude. This can be achieved by protein engineering to increase calcium and Mn^{2+} binding affinities (in the calcium-bound state), ideally to sub-μM K_d(s). Improved Mn^{2+} binding will also have the added advantage of minimizing competition from other Mn^{2+} sequestering molecules such as ATP and certain proteins (e.g., glutamine synthetase), which typically exhibit weaker but non-negligible Mn^{2+} affinity (~tens of μM) compared to calprotectin.[73] These efforts are likely to benefit from the ability to utilize molecular engineering techniques such as directed evolution, which have been remarkably successful in expanding the toolbox

of fluorescent calcium indicators[10] as well as developing new MRI reporters based on metalloproteins.[42,74–77] In summary, as the first biomolecular reporter for sensing calcium by MRI, calprotectin is a promising step in the ambitious path toward understanding how neural circuits and networks distributed throughout the mammalian brain coordinate to process information and generate behavior.

Supplementary Material

Refer to Web version on PubMed Central for supplementary material.

ACKNOWLEDGMENTS

We thank members of the Mukherjee lab for helpful discussions. We are grateful to Prof. Elizabeth Nolan (MIT) for introducing us to calprotectins. We thank Prof. Mikhail Shapiro (Caltech) for insightful discussions on MRI and calcium imaging. This work was supported by the California NanoSystems Institute (University of California, Santa Barbara), a NARSAD Young Investigator Award from the Brain and Behavior Research Foundation, and a National Institutes of Health R35 Maximizing Investigators' Research Award (MIRA) and an R03 Imaging – Science Track Award for Research Transition (I/STAR) (to AM). HFO gratefully acknowledges support from the Errett Fisher Foundation. Finally, we extend our gratitude to the anonymous reviewers whose thorough analysis greatly helped in strengthening this work.

REFERENCES

(1). Simons TJB Calcium and neuronal function. Neurosurg. Rev 1988, 11, 119–129. [PubMed: 2854227]

(2). Brini M; Cali T; Ottolini D; Carafoli E Neuronal calcium signaling: function and dysfunction. Cell. Mol. Life Sci 2014, 71 (15), 2787–814. [PubMed: 24442513]

(3). Grienberger C; Konnerth A Imaging calcium in neurons. Neuron 2012, 73 (5), 862–885. [PubMed: 22405199]

(4). Wang W; Kim CK; Ting AY Molecular tools for imaging and recording neuronal activity. Nat. Chem. Biol 2019, 15 (2), 101–110. [PubMed: 30659298]

(5). Tian L; Akerboom J; Schreiter ER; Looger LL Neural activity imaging with genetically encoded calcium indicators. Prog. Brain Res 2012, 196, 79–94. [PubMed: 22341322]

(6). Qian Y; Piatkevich KD; Mc Larney B; Abdelfattah AS; Mehta S; Murdock MH; Gottschalk S; Molina RS; Zhang W; Chen Y A genetically encoded near-infrared fluorescent calcium ion indicator. Nat. Methods 2019, 16 (2), 171–174. [PubMed: 30664778]

(7). Nakai J; Ohkura M; Imoto K A high signal-to-noise Ca 2+ probe composed of a single green fluorescent protein. Nat. Biotechnol 2001, 19 (2), 137–141. [PubMed: 11175727]

(8). Dana H; Sun Y; Mohar B; Hulse BK; Kerlin AM; Hasseman JP; Tsegaye G; Tsang A; Wong A; Patel R High-performance calcium sensors for imaging activity in neuronal populations and microcompartments. Nat. Methods 2019, 16 (7), 649–657. [PubMed: 31209382]

(9). Zhao Y; Araki S; Wu J; Teramoto T; Chang Y-F; Nakano M; Abdelfattah AS; Fujiwara M; Ishihara T; Nagai T An expanded palette of genetically encoded Ca2+ indicators. Science 2011, 333 (6051), 1888–1891. [PubMed: 21903779]

(10). Shen Y; Nasu Y; Shkolnikov I; Kim A; Campbell RE Engineering genetically encoded fluorescent indicators for imaging of neuronal activity: Progress and prospects. Neurosci. Res 2020, 152, 3–14. [PubMed: 31991206]

(11). Chen T-W; Wardill TJ; Sun Y; Pulver SR; Renninger SL; Baohan A; Schreiter ER; Kerr RA; Orger MB; Jayaraman V; Looger LL; Svoboda K; Kim DS Ultrasensitive fluorescent proteins for imaging neuronal activity. Nature 2013, 499 (7458), 295–300. [PubMed: 23868258]

(12). Tian L; Hires SA; Mao T; Huber D; Chiappe ME; Chalasani SH; Petreanu L; Akerboom J; McKinney SA; Schreiter ER Imaging neural activity in worms, flies and mice with improved GCaMP calcium indicators. Nat. Methods 2009, 6 (12), 875–881. [PubMed: 19898485]

(13). Miyawaki A; Llopis J; Heim R; McCaffery JM; Adams JA; Ikura M; Tsien RY Fluorescent indicators for Ca 2+ based on green fluorescent proteins and calmodulin. Nature 1997, 388 (6645), 882–887. [PubMed: 9278050]

(14). Qian Y; Rancic V; Wu J; Ballanyi K; Campbell RE A bioluminescent Ca2+ indicator based on a topological variant of GCaMP6s. ChemBioChem 2019, 20 (4), 516–520. [PubMed: 29934970]

(15). Akerboom J; Chen T-W; Wardill TJ; Tian L; Marvin JS; Mutlu S; Calderón NC; Esposti F; Borghuis BG; Sun XR; et al. Optimization of a GCaMP calcium indicator for neural activity imaging. J. Neurosci 2012, 32 (40), 13819–13840. [PubMed: 23035093]

(16). Heim N; Griesbeck O Genetically encoded indicators of cellular calcium dynamics based on troponin C and green fluorescent protein. J. Biol. Chem 2004, 279 (14), 14280–6. [PubMed: 14742421]

(17). Stirman JN; Smith IT; Kudenov MW; Smith SL Wide field-of-view, multi-region, two-photon imaging of neuronal activity in the mammalian brain. Nat. Biotechnol 2016, 34 (8), 857–862. [PubMed: 27347754]

(18). Ji N; Freeman J; Smith SL Technologies for imaging neural activity in large volumes. Nat. Neurosci 2016, 19 (9), 1154. [PubMed: 27571194]

(19). Kim TH; Zhang Y; Lecoq J; Jung JC; Li J; Zeng H; Niell CM; Schnitzer MJ Long-term optical access to an estimated one million neurons in the live mouse cortex. Cell Rep. 2016, 17 (12), 3385–3394. [PubMed: 28009304]

(20). Scott BB; Thiberge SY; Guo C; Tervo DGR; Brody CD; Karpova AY; Tank DW Imaging cortical dynamics in GCaMP transgenic rats with a head-mounted widefield macroscope. Neuron 2018, 100 (5), 1045–1058. [PubMed: 30482694]

(21). Cui G; Jun SB; Jin X; Luo G; Pham MD; Lovinger DM; Vogel SS; Costa RM Deep brain optical measurements of cell type–specific neural activity in behaving mice. Nat. Protoc 2014, 9 (6), 1213–1228. [PubMed: 24784819]

(22). Ghosh KK; Burns LD; Cocker ED; Nimmerjahn A; Ziv Y; El Gamal A; Schnitzer MJ Miniaturized integration of a fluorescence microscope. Nat. Methods 2011, 8 (10), 871. [PubMed: 21909102]

(23). Li W.-h.; Fraser SE; Meade TJ A Calcium-Sensitive Magnetic Resonance Imaging Contrast Agent. J. Am. Chem. Soc 1999, 121, 1413–1414.

(24). Atanasijevic T; Shusteff M; Fam P; Jasanoff A Calcium-sensitive MRI contrast agents based on superparamagnetic iron oxide nanoparticles and calmodulin. Proc. Natl. Acad. Sci. U. S. A 2006, 103 (40), 14707–12. [PubMed: 17003117]

(25). Angelovski G; Fouskova P; Mamedov I; Canals S; Toth E; Logothetis NK Smart magnetic resonance imaging agents that sense extracellular calcium fluctuations. ChemBioChem 2008, 9 (11), 1729–34. [PubMed: 18604834]

(26). Mamedov I; Canals S; Henig J; Beyerlein M; Murayama Y; Mayer HA; Logothetis NK; Angelovski G In vivo characterization of a smart MRI agent that displays an inverse response to calcium concentration. ACS Chem. Neurosci 2010, 1 (12), 819–28. [PubMed: 22778817]

(27). Angelovski G; Chauvin T; Pohmann R; Logothetis NK; Toth E Calcium-responsive paramagnetic CEST agents. Bioorg. Med. Chem 2011, 19 (3), 1097–105. [PubMed: 20691598]

(28). Bar-Shir A; Gilad AA; Chan KW; Liu G; van Zijl PC; Bulte JW; McMahon MT Metal ion sensing using ion chemical exchange saturation transfer 19F magnetic resonance imaging. J. Am. Chem. Soc 2013, 135 (33), 12164–7. [PubMed: 23905693]

(29). Angelovski G; Gottschalk S; Milosevic M; Engelmann J; Hagberg GE; Kadjane P; Andjus P; Logothetis NK Investigation of a calcium-responsive contrast agent in cellular model systems: feasibility for use as a smart molecular probe in functional MRI. ACS Chem. Neurosci 2014, 5 (5), 360–9. [PubMed: 24712900]

(30). Bar-Shir A; Avram L; Yariv-Shoushan S; Anaby D; Cohen S; Segev-Amzaleg N; Frenkel D; Sadan O; Offen D; Cohen Y Alginate-coated magnetic nanoparticles for noninvasive MRI of extracellular calcium. NMR Biomed. 2014, 27 (7), 774–83. [PubMed: 24764262]

(31). Garello F; Vibhute S; Gunduz S; Logothetis NK; Terreno E; Angelovski G Innovative Design of Ca-Sensitive Paramagnetic Liposomes Results in an Unprecedented Increase in Longitudinal Relaxivity. Biomacromolecules 2016, 17 (4), 1303–11. [PubMed: 26956911]

(32). MacRenaris KW; Ma Z; Krueger RL; Carney CE; Meade TJ Cell-Permeable Esterase-Activated Ca(II)-Sensitive MRI Contrast Agent. Bioconjugate Chem. 2016, 27 (2), 465–73.

(33). Preslar AT; Lilley LM; Sato K; Zhang S; Chia ZK; Stupp SI; Meade TJ Calcium-Induced Morphological Transitions in Peptide Amphiphiles Detected by (19)F-Magnetic Resonance Imaging. ACS Appl. Mater. Interfaces 2017, 9 (46), 39890–39894. [PubMed: 28915004]

(34). Okada S; Bartelle BB; Li N; Breton-Provencher V; Lee JJ; Rodriguez E; Melican J; Sur M; Jasanoff A Calcium-dependent molecular fMRI using a magnetic nanosensor. Nat. Nanotechnol 2018, 13 (6), 473–477. [PubMed: 29713073]

(35). Barandov A; Bartelle BB; Williamson CG; Loucks ES; Lippard SJ; Jasanoff A Sensing intracellular calcium ions using a manganese-based MRI contrast agent. Nat. Commun 2019, 10 (1), 897. [PubMed: 30796208]

(36). Du K; Thorarinsdottir AE; Harris TD Selective Binding and Quantitation of Calcium with a Cobalt-Based Magnetic Resonance Probe. J. Am. Chem. Soc 2019, 141 (17), 7163–7172. [PubMed: 30946580]

(37). Adams CJ; Krueger R; Meade TJ A Multimodal Ca(II) Responsive Near IR-MR Contrast Agent Exhibiting High Cellular Uptake. ACS Chem. Biol 2020, 15 (2), 334–341. [PubMed: 31967770]

(38). Gambino G; Gambino T; Pohmann R; Angelovski G A ratiometric (19)F MR-based method for the quantification of Ca(2+) using responsive paramagnetic probes. Chem. Commun. (Cambridge, U.K.) 2020, 56 (24), 3492–3495.

(39). Garello F; Gunduz S; Vibhute S; Angelovski G; Terreno E Dendrimeric calcium-sensitive MRI probes: the first low-field relaxometric study. J. Mater. Chem. B 2020, 8 (5), 969–979. [PubMed: 31930247]

(40). Miller ADC; Ozbakir HF; Mukherjee A Calcium-responsive contrast agents for functional magnetic resonance imaging. Chemical Physics Reviews 2021, 2 (2), 021301. [PubMed: 34085055]

(41). Shapiro MG; Szablowski JO; Langer R; Jasanoff A Protein nanoparticles engineered to sense kinase activity in MRI. J. Am. Chem. Soc 2009, 131 (7), 2484–6. [PubMed: 19199639]

(42). Shapiro MG; Westmeyer GG; Romero PA; Szablowski JO; Kuster B; Shah A; Otey CR; Langer R; Arnold FH; Jasanoff A Directed evolution of a magnetic resonance imaging contrast agent for noninvasive imaging of dopamine. Nat. Biotechnol 2010, 28 (3), 264–70. [PubMed: 20190737]

(43). Hsieh V; Okada S; Wei H; García-Álvarez I; Barandov A; Alvarado SR; Ohlendorf R; Fan J; Ortega A; Jasanoff A Neurotransmitter-responsive nanosensors for T 2-weighted magnetic resonance imaging. J. Am. Chem. Soc 2019, 141 (40), 15751–15754. [PubMed: 31523957]

(44). Brustad EM; Lelyveld VS; Snow CD; Crook N; Jung ST; Martinez FM; Scholl TJ; Jasanoff A; Arnold FH Structure-guided directed evolution of highly selective p450-based magnetic resonance imaging sensors for dopamine and serotonin. J. Mol. Biol 2012, 422 (2), 245–62. [PubMed: 22659321]

(45). Hai A; Cai LX; Lee T; Lelyveld VS; Jasanoff A Molecular fMRI of serotonin transport. Neuron 2016, 92 (4), 754–765. [PubMed: 27773583]

(46). Lee T; Cai LX; Lelyveld VS; Hai A; Jasanoff A Molecular-level functional magnetic resonance imaging of dopaminergic signaling. Science 2014, 344 (6183), 533–535. [PubMed: 24786083]

(47). Corbin BD; Seeley EH; Raab A; Feldmann J; Miller MR; Torres VJ; Anderson KL; Dattilo BM; Dunman PM; Gerads R Metal chelation and inhibition of bacterial growth in tissue abscesses. Science 2008, 319 (5865), 962–965. [PubMed: 18276893]

(48). Kehl-Fie TE; Chitayat S; Hood MI; Damo S; Restrepo N; Garcia C; Munro KA; Chazin WJ; Skaar EP Nutrient metal sequestration by calprotectin inhibits bacterial superoxide defense, enhancing neutrophil killing of Staphylococcus aureus. Cell Host Microbe 2011, 10 (2), 158–64. [PubMed: 21843872]

(49). Zackular JP; Chazin WJ; Skaar EP Nutritional immunity: S100 proteins at the host-pathogen interface. J. Biol. Chem 2015, 290 (31), 18991–18998. [PubMed: 26055713]

(50). Brophy MB; Nolan EM Manganese and microbial pathogenesis: sequestration by the Mammalian immune system and utilization by microorganisms. ACS Chem. Biol 2015, 10 (3), 641–651. [PubMed: 25594606]

(51). Brunjes Brophy M; Nakashige TG; Gaillard A; Nolan EM Contributions of the S100A9 C-terminal tail to high-affinity Mn (II) chelation by the host-defense protein human calprotectin. J. Am. Chem. Soc 2013, 135 (47), 17804–17817. [PubMed: 24245608]

(52). Damo SM; Kehl-Fie TE; Sugitani N; Holt ME; Rathi S; Murphy WJ; Zhang Y; Betz C; Hench L; Fritz G Molecular basis for manganese sequestration by calprotectin and roles in the innate immune response to invading bacterial pathogens. Proc. Natl. Acad. Sci. U. S. A 2013, 110 (10), 3841–3846. [PubMed: 23431180]

(53). Zygiel EM; Nolan EM Transition Metal Sequestration by the Host-Defense Protein Calprotectin. Annu. Rev. Biochem 2018, 87, 621–643. [PubMed: 29925260]

(54). Korndörfer IP; Brueckner F; Skerra A The crystal structure of the human (S100A8/S100A9) 2 heterotetramer, calprotectin, illustrates how conformational changes of interacting α-helices can determine specific association of two EF-hand proteins. J. Mol. Biol 2007, 370 (5), 887–898. [PubMed: 17553524]

(55). Gagnon DM; Brophy MB; Bowman SE; Stich TA; Drennan CL; Britt RD; Nolan EM Manganese binding properties of human calprotectin under conditions of high and low calcium: X-ray crystallographic and advanced electron paramagnetic resonance spectroscopic analysis. J. Am. Chem. Soc 2015, 137 (8), 3004–16. [PubMed: 25597447]

(56). Hayden JA; Brophy MB; Cunden LS; Nolan EM High-affinity manganese coordination by human calprotectin is calcium-dependent and requires the histidine-rich site formed at the dimer interface. J. Am. Chem. Soc 2013, 135 (2), 775–87. [PubMed: 23276281]

(57). Caravan P; Farrar CT; Frullano L; Uppal R Influence of molecular parameters and increasing magnetic field strength on relaxivity of gadolinium-and manganese-based T1 contrast agents. Contrast Media Mol. Imaging 2009, 4 (2), 89–100. [PubMed: 19177472]

(58). Li N; Jasanoff A Local and global consequences of reward-evoked striatal dopamine release. Nature 2020, 580 (7802), 239–244. [PubMed: 32269346]

(59). Mukherjee A; Wu D; Davis HC; Shapiro MG Noninvasive imaging using reporter genes altering cellular water permeability. Nat. Commun 2016, 7 (1), 13891. [PubMed: 28008959]

(60). Albaugh DL; Salzwedel A; Van Den Berge N; Gao W; Stuber GD; Shih Y-YI Functional Magnetic Resonance Imaging of Electrical and Optogenetic Deep Brain Stimulation at the Rat Nucleus Accumbens. Sci. Rep 2016, 6 (1), 31613. [PubMed: 27601003]

(61). Rao W; Peng C; Zhang L; Su N; Wang K; Hui H; Dai S.-h.; Yang Y.-f.; Luo P; Fei Z Homer1a attenuates glutamate-induced oxidative injury in HT-22 cells through regulation of store-operated calcium entry. Sci. Rep 2016, 6 (1), 33975. [PubMed: 27681296]

(62). Zhang X; Qiao Z; Liu N; Gao L; Wei L; Liu A; Ma Z; Wang F; Hou S; Li J; Shen H Stereotypical patterns of epileptiform calcium signal in hippocampal CA1, CA3, dentate gyrus and entorhinal cortex in freely moving mice. Sci. Rep 2019, 9 (1), 4518. [PubMed: 30872744]

(63). Daoust A; Barbier EL; Bohic S; Stupar V; Maunoir-Regimbal S; Fauvelle F Impact of manganese on the hippocampus metabolism in the context of MEMRI: a proton HRMAS MRS study. Toxicol. Res 2015, 4 (2), 376–384.

(64). Silva AC; Lee JH; Aoki I; Koretsky AP Manganese-enhanced magnetic resonance imaging (MEMRI): methodological and practical considerations. NMR Biomed. 2004, 17 (8), 532–543. [PubMed: 15617052]

(65). Jacobs KE; Behera D; Rosenberg J; Gold G; Moseley M; Yeomans D; Biswal S Oral manganese as an MRI contrast agent for the detection of nociceptive activity. NMR Biomed. 2012, 25 (4), 563–569. [PubMed: 22447731]

(66). Atanasijevic T; Bouraoud N; McGavern DB; Koretsky AP Transcranial manganese delivery for neuronal tract tracing using MEMRI. NeuroImage 2017, 156, 146–154. [PubMed: 28506873]

(67). Silva AC; Lee JH; Aoki I; Koretsky AP Manganese-enhanced magnetic resonance imaging (MEMRI): methodological and practical considerations. NMR Biomed. 2004, 17 (8), 532–43. [PubMed: 15617052]

(68). Koretsky AP; Silva AC Manganese-enhanced magnetic resonance imaging (MEMRI); Wiley Online Library: 2004.

(69). Malkova NV; Gallagher JJ; Collin ZY; Jacobs RE; Patterson PH Manganese-enhanced magnetic resonance imaging reveals increased DOI-induced brain activity in a mouse model

of schizophrenia. Proc. Natl. Acad. Sci. U. S. A 2014, 111 (24), E2492–E2500. [PubMed: 24889602]

(70). Lu H; Xi Z-X; Gitajn L; Rea W; Yang Y; Stein EA Cocaine-induced brain activation detected by dynamic manganese-enhanced magnetic resonance imaging (MEMRI). Proc. Natl. Acad. Sci. U. S. A 2007, 104 (7), 2489–2494. [PubMed: 17287361]

(71). Bartelle BB; Mana MD; Suero-Abreu GA; Rodriguez JJ; Turnbull DH Engineering an effective Mn-binding MRI reporter protein by subcellular targeting. Magn. Reson. Med 2015, 74 (6), 1750–1757. [PubMed: 25522343]

(72). Bartelle BB; Szulc KU; Suero-Abreu GA; Rodriguez JJ; Turnbull DH Divalent metal transporter, DMT1: A novel MRI reporter protein. Magn. Reson. Med 2013, 70 (3), 842–850. [PubMed: 23065715]

(73). Fanali G; Cao Y; Ascenzi P; Fasano M Mn (II) binding to human serum albumin: a 1H-NMR relaxometric study. J. Inorg. Biochem 2012, 117, 198–203. [PubMed: 23099538]

(74). Liu X; Lopez PA; Giessen TW; Giles M; Way JC; Silver PA Engineering Genetically-Encoded Mineralization and Magnetism via Directed Evolution. Sci. Rep 2016, 6 (1), 38019. [PubMed: 27897245]

(75). Matsumoto Y; Chen R; Anikeeva P; Jasanoff A Engineering intracellular biomineralization and biosensing by a magnetic protein. Nat. Commun 2015, 6 (1), 8721. [PubMed: 26522873]

(76). Brustad EM; Lelyveld VS; Snow CD; Crook N; Jung ST; Martinez FM; Scholl TJ; Jasanoff A; Arnold FH Structure-Guided Directed Evolution of Highly Selective P450-Based Magnetic Resonance Imaging Sensors for Dopamine and Serotonin. J. Mol. Biol 2012, 422 (2), 245–262. [PubMed: 22659321]

(77). Xue S; Yang H; Qiao J; Pu F; Jiang J; Hubbard K; Hekmatyar K; Langley J; Salarian M; Long RC Protein MRI contrast agent with unprecedented metal selectivity and sensitivity for liver cancer imaging. Proc. Natl. Acad. Sci. U. S. A 2015, 112 (21), 6607–6612. [PubMed: 25971726]

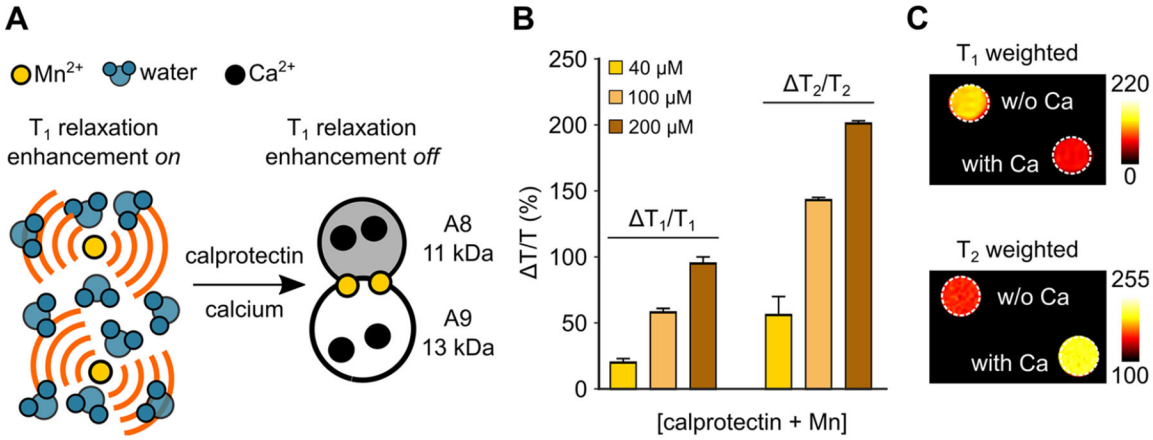

Figure 1.

Principle of calcium imaging with calprotectins. (A) Proposed mechanism of MRI contrast induced by sequestration of paramagnetic Mn^{2+} ions by calprotectin in the presence of calcium. (B) Percent change in T_1 and T_2 relaxation times obtained for a binary mixture of calprotectin (40, 100, and 200 μM) and Mn^{2+} (30, 75, and 150 μM) in response to saturating amounts of calcium (2 mM) in HEPES buffer 9; pH 7.4). (C) T_1 and T_2 weighted images of calcium (2 mM) induced MRI contrast obtained with a binary mixture of 200 μM calprotectin and 150 μM Mn^{2+}. All MRI measurements were performed at 7 T. Error bars represent standard error of mean from 5 independent replicates.

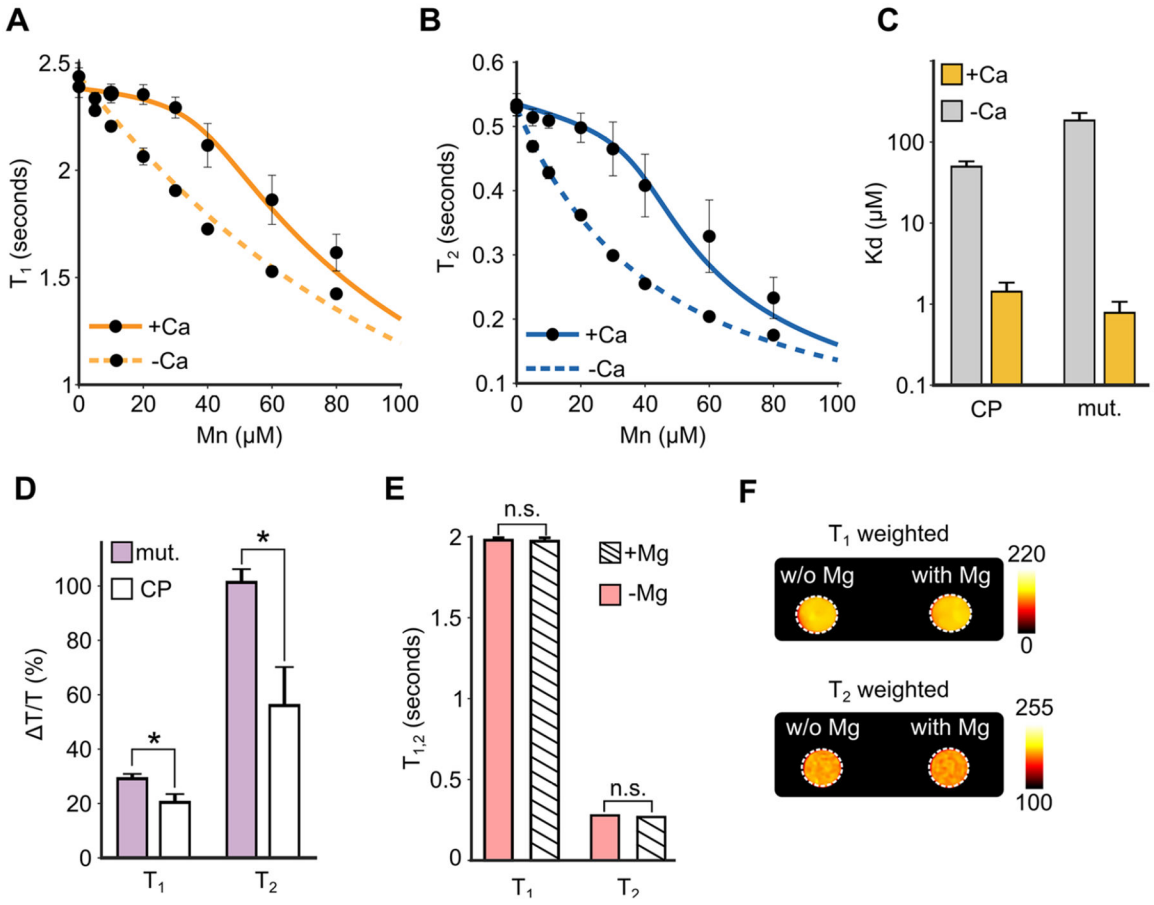

Figure 2.

In vitro MRI relaxometry of calprotectin-based Ca^{2+} sensors. In the presence of calcium (2 mM), (A) T_1 and (B) T_2 relaxation times exhibit a significantly smaller decrease with increasing Mn^{2+} concentrations due to Mn^{2+} sequestration by calprotectin. The solid lines represent best fits to equilibrium binding isotherms. (C) Dissociation constants for Mn^{2+} binding to calprotectin (CP) and His_3Asp variant (mut.) in the presence and absence of saturating calcium (2 mM), estimated from model-fitting of T_1 titration results. (D) Calcium-induced percent change in T_1 and T_2 for calprotectin and the His_3Asp mutant. (E) Calprotectin does not produce a change in T_1 and T_2 values or (F) detectable T_1 and T_2 weighted MRI contrast in response to saturating amounts of Mg^{2+} (2 mM). For all experiments, protein and calcium concentrations were 40 μM and 2 mM, respectively. Mn^{2+} was either titrated from 0 to 30 μM (A,B) or used at 30 μM (D–F). Relaxation rates were measured at 7 T. Error bars represent standard error of mean from 3–5 independent replicates. * denotes $p < 0.05$ and n.s. indicates $p > 0.05$ (Student's *t* test).

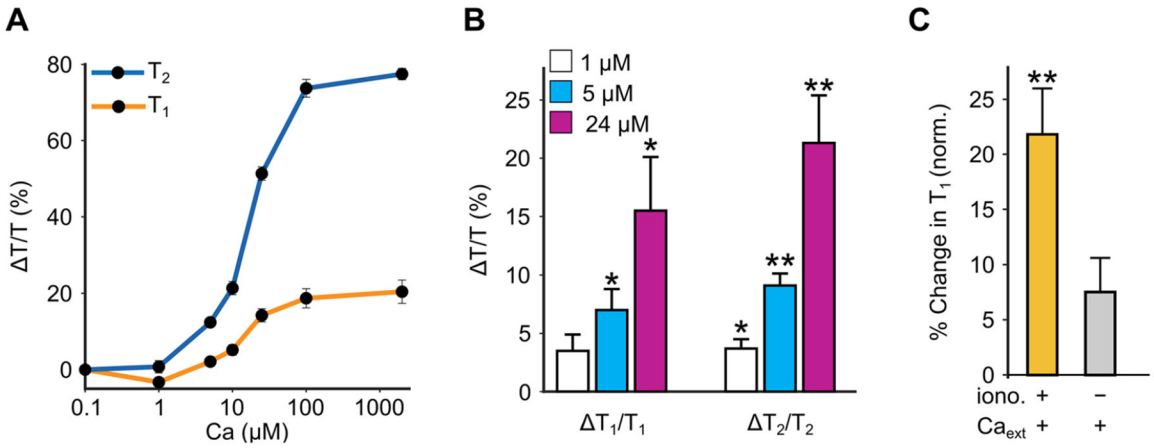

Figure 3.

MRI-based sensing of biologically relevant calcium concentrations. (A) Percent change in T_1 and T_2 relaxation times in response to calcium concentrations spanning 0.1 μM to 1 mM. Calprotectin and Mn^{2+} concentrations were 40 μM and 30 μM, respectively. (B) Percent change in relaxation times obtained by adding calprotectin (40 μM) and Mn^{2+} (30 μM) to a hippocampal cell lysate preparation treated with biologically relevant concentrations of calcium (1, 5, and 24 μM). (C) Change in T_1 elicited by stimulating calcium entry in Chinese hamster ovary (CHO) cells lentivirally transduced with calprotectin-expressing vectors and treated with 10 μM calcimycin, a calcium ionophore. As ionophore treatment by itself alters cellular T_1, all values are normalized to T_1 values measured concurrently in identically treated CHO cells that have not been transduced to express calprotectin. Relaxation rates were measured at 7 T. Error bars represent standard error of mean from 3–5 independent replicates. * denotes $p < 0.05$ and ** indicates $p < 0.01$ (Student's t test).